
ResT V2: Simpler, Faster and Stronger

Qing-Long Zhang, Yu-Bin Yang
 State Key Laboratory for Novel Software Technology
 Nanjing University, Nanjing 21023, China
 wofmanaf@mail.nju.edu.cn, yangyubin@nju.edu.cn

Abstract

This paper proposes ResTv2, a simpler, faster, and stronger multi-scale vision Transformer for visual recognition. ResTv2 simplifies the EMSA structure in ResTv1 (i.e., eliminating the multi-head interaction part) and employs an upsample operation to reconstruct the lost medium- and high-frequency information caused by the downsampling operation. In addition, we explore different techniques for better apply ResTv2 backbones to downstream tasks. We find that although combining EMSAv2 and window attention can greatly reduce the theoretical matrix multiply FLOPs, it may significantly decrease the computation density, thus causing lower actual speed. We comprehensively validate ResTv2 on ImageNet classification, COCO detection, and ADE20K semantic segmentation. Experimental results show that the proposed ResTv2 can outperform the recently state-of-the-art backbones by a large margin, demonstrating the potential of ResTv2 as solid backbones. The code and models will be made publicly available at <https://github.com/wofmanaf/Rest>.

1 Introduction

Recent advances in Vision Transformers (ViTs) have created new state-of-the-art results on many computer vision tasks. While scaling up ViTs with billions of parameters [22, 9, 45, 40, 13] is a well-proven way to improve the capacity of the ViTs, it is more important to explore more energy-efficient approaches to build simpler ViTs with fewer parameters and less computation cost while retaining high model capacity.

Toward this direction, there are a few works that significantly improve the efficiency of ViTs [35, 10, 12, 23, 5]. The first kind is reintroducing the “sliding window” strategy to ViTs. Among them, Swin Transformer [23] is a milestone work that partitions the patched inputs into non-overlapping windows and computes multi-head self-attention (MSA) independently within each window. Based on Swin, Focal Transformer [41] further splits the feature map into multiple windows in which tokens share the same surroundings to effectively capture short- and long-range dependencies. The second type to improve efficiency is downsampling one or several dimension of MSA. PVT [35] is a pioneer work in this area, which adopts another non-overlapping patch embedding module to reduce the spatial dimension of keys and values in MSA. ResTv1 [47] further explores three types of overlapping spatial reduction methods (i.e., max pooling, average pooling, and depth-wise convolution) in MSA to balance the computation and effectiveness in different scenarios. However, the downsampling operation in MSA will inevitably impair the model’s performance since it destroys the global dependency modeling ability of MSA to a certain extent (shown in Figure 1).

In this paper, we propose EMSAv2, which explores different upsample strategies adding to EMSA to compensate for the performance degradation caused by the downsampling operation. Surprisingly, the “downsample-upsample” combination happens to build an independent convolution branch, which can reconstruct the lost information with fewer extra parameters and computation costs. Besides, EMSAv2 eliminates the multi-head interaction module in EMSA to simply the self-attention structure.

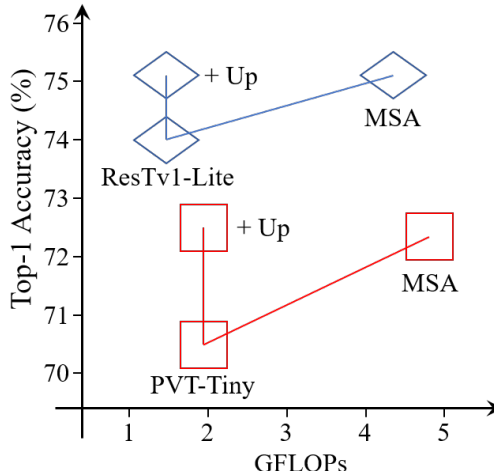


Figure 1: Top-1 Accuracy of ResT-Lite [47] and PVT-Tiny [35] under 100 epochs training settings. Results show that downsampling operation will impair the performance while adding an upsampling operation can address this issue. Detailed comparisons are shown in Appendix A.

Based on EMSAv2, we build simpler, faster, and stronger general-purpose backbones, ResTv2. In addition, we explore four methods of applying ResTv2 backbones to downstream tasks. We found that combining EMSAv2 and window attention is not that good when the inputs’ resolution is high (e.g., 800×1333), although it can significantly reduce the theoretical matrix multiply FLOPs. Due to the padding operation in window partition and grouping operation of window attention, the computation density of EMSAv2 will be significantly decreased, causing lower actual inference speed. We hope the observations and discussions can challenge some common beliefs and encourage people to rethink the relations between theoretical FLOPs and actual speeds, particularly running on GPUs.

We evaluate ResTv2 on various vision tasks such as ImageNet classification, object detection/segmentation on COCO, and semantic segmentation on ADE20K. Experimental results reveal the potential of ResTv2 as strong backbones. For example, our ResTv2-L yields 84.2% Top-1 accuracy (with size 224^2) on ImageNet-1k, which is significantly better than Swin-B [23] (83.5%) and ConvNeXt-B [24] (83.8%), while ResTv2-L has fewer parameters (87M vs. 88M vs. 89M) and much higher throughput (415 vs. 278 vs. 292 images/s).

2 Related Work

Efficient self-attention structures. MSA has shown great power to capture global dependency in computer vision tasks [11, 2, 3, 43, 43, 50]. However, the computation complexity of MSA is quadratic to the input size, which might be acceptable for ImageNet classification, but quickly becomes intractable with higher-resolution inputs. One typical way to improve efficiency is partitioning the patched inputs into non-overlapping windows and computing self-attention independently within each of these windows (i.e., windowed self-attention). To enable information communicate across windows, researchers have developed several integrate techniques, such as shift window [23], spatial shuffle [17], or alternately running global attention and local attention [5, 42] between successive blocks. Other ways are trying to reduce spatial dimension of the MSA. For example, PVT [35] and ResTv1 [47] designed different downsample strategies to reduce the spatial dimension of keys and values in MSA. MViT [12] proposed pooling attention to downsample queries, keys, and values spatial resolution. However, either the windowed self-attention or downsampled self-attention will impair the long-distance modeling ability to some content, i.e., surrendering some important information for efficiency. Our target in this paper is to reconstruct the lost information in a light way.

Convolution enhanced MSA. Recently, designing transformer models with convolution operations has become popular since convolutions can introduce inductive biases, which is complementary to MSA. ResTv1 [47] and [38] reintroduce convolutions at the early stage to achieve stabler training.

CoAtNet [9] and UniFormer [19] replace MSA blocks with convolution blocks in the former two stages. CvT [36] adopts convolution in the tokenization process and utilizes stride convolution to reduce the computation complexity of self-attention. CSwin Transformer [10] and CPVT [6] adopt a convolution-based positional encoding technique and show improvements on downstream tasks. Conformer [28] and Mobile-Former[4] combine Transformer with an independent ConvNet model to fuse convolutional features and MSA representations under different resolutions. ACmix [26] explores a closer relationship between convolution and self-attention by sharing the 1×1 convolutions and combining them with the remaining lightweight aggregation operations. The “downsample-upsample” branch in ResTv2 happens to build an independent convolutional module, which can effectively reconstruct information lost by the MSA module.

3 Proposed Method

3.1 A brief review of ResTv1

ResTv1[47] is an efficient multi-scale vision Transformer, which can capably serve as a general-purpose backbone for image recognition. ResTv1 effectively reduces the memory of standard MSA [34, 11] and models the interaction between multi-heads while keeping the diversity ability. To tackle input images with an arbitrary size, ResTv1 constructs the positional embedding as spatial attention, which models absolute positions between pixels with the help of zero paddings in the transformation function.

EMSA is the critical component in ResTv1 [47] (shown in Figure 2(a)). Given a 1D input token $x \in \mathbb{R}^{n \times d_m}$, where n is the token length, d_m is the channel dimension. EMSA first projects x using a linear operation to get the query: $Q = xW_q + b_q$, where W_q and b_q are the weights and bias of linear projection. After that, Q is split into k groups (i.e., k heads) to prepare for the next step, i.e., $Q \in \mathbb{R}^{k \times n \times d_k}$, where $d_k = d_m/k$ is the head dimension. To compress memory, x is reshaped to its 2D size and then are downsampled by a depth-wise convolution to reduce the height and width. After that, the output x' is reshaped to the 1D size, and then a Layer Norm [1] is added. Then the author employs the same way as to obtain Q to get key K and value V on x' . The output of EMSA can be calculated by

$$\text{EMSA}(Q, K, V) = \text{Norm}(\text{Softmax}(\text{Conv}(\frac{QK^T}{\sqrt{d_k}})))V \quad (1)$$

where “Conv” is applied to model the interactions among different heads. “Norm” can be Instance Norm [33] or Layer Norm [1], which is applied to re-weight the attention matrix captured by different heads.

3.2 ResTv2

As shown in Figure 1, although downsample operation in EMSA can significantly reduce the computation cost, it will inevitably lose some vital information, particularly in the earlier stages, where the downsampling ratio is relatively higher, e.g., 8 in the first stage. To address this issue, one feasible solution is to introduce spatial pyramid structural information. That is, setting different downsampling rates for the input, calculating the corresponding keys and values respectively, and then combining these multi-scale keys and values along the channel dimension. The obtained new keys and values are then sent to the EMSA module to model global dependencies or directly calculate multi-scale self-attention with the original multi-scale keys and values.

However, the multi-path calculation of keys and values will greatly reduce the computational density of self-attention, although the theoretical FLOPs do not seem to change much. For example, the multi-path Focal-T [41] and the single-path Swin-T [23] have comparable theoretical FLOPs (4.9G vs. 4.5G), but the actual inference throughput of Focal-T is only 0.42 times of Swin-T (319 vs. 755 images/s).

In order to effectively reconstruct the lost information without having a large impact on the actual running speed, in this paper, we propose to execute an upsampling operation on the values directly. There are many upsampling strategies, such as “nearest”, “bilinear”, “pixel-shuffle”, etc. We find that all of them can improve the model’s performance, but “pixel-shuffle” works better. We call this new self-attention structure EMSAv2. The detailed structure is shown in Figure 2(b).

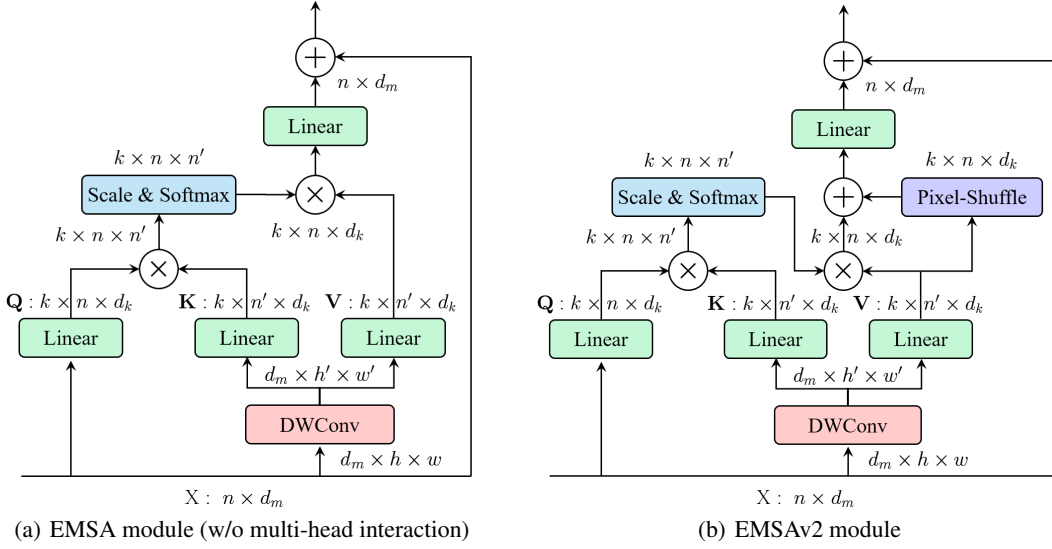


Figure 2: Comparison of EMSA in ResTv1 and EMSAv2 in ResTv2. To simplify, the “multi-head interaction” module in EMSA is not displayed.

Surprisingly, the “downsample-upsample” combination in EMSAv2 happens to build an independent convolution branch, which can efficiently reconstruct the lost information with fewer extra parameters and computation costs. Besides, we find that the multi-head interaction module of the self-attention branch in EMSAv2 will decrease the actual inference speed of EMSAv2, although it can increase the final performance. And the performance improvements will be decreased as the channel dimension for each head increases. Therefore, we remove it for faster speed under default settings. However, if the head dimension is small (e.g., $d_k = 64$ or smaller), the multi-head interaction module will make a difference (Detailed Results can be found in Appendix B). By doing so, we can also increase the training speed since the computation gap between the self-attention branch and the upsample branch is reduced. The mathematical definition of the EMSAv2 module can be represented as

$$\text{EMSA}(Q, K, V) = \text{Softmax}\left(\frac{QK^T}{\sqrt{d_k}}\right)V + \text{Up}(V) \quad (2)$$

3.3 Model configurations.

We construct different ResTv2 variants based on EMSAv2. ResTv2-T/B/L, to be of similar complexities to Swin-T/S/B. We also build ResTv2-S to make a better speed-accuracy trade-off. The four variants only differ in the number of channels, heads’ number of EMSAv2, and blocks in each stage. Other hyper-parameters are the same as ResTv1[47]. Note that the upsampling module in ResTv2 introduces extra parameters and FLOPs. To make a fair comparison, the block number in the first stage of ResTv2-T/S/B is set to 1, half of the one in ResTv1. Assume C is the channel number of hidden layers in the first stage. We summarize the configurations below:

- ResTv2-T: $C = 96$, heads = {1, 2, 4, 8}, blocks number = {1, 2, 6, 2}
- ResTv2-S: $C = 96$, heads = {1, 2, 4, 8}, blocks number = {1, 2, 12, 2}
- ResTv2-B: $C = 96$, heads = {1, 2, 4, 8}, blocks number = {1, 3, 16, 3}
- ResTv2-L: $C = 128$, heads = {2, 4, 8, 16}, blocks number = {2, 3, 16, 2}

Detailed model size, theoretical computational complexity (FLOPs), and hyper-parameters of the model variants for ImageNet image classification are listed in Appendix D.

3.4 Explanation of upsample branch

To better explain the role of the upsample branch in EMSAv2, we plot the Fourier transformed feature maps of EMSAv2, the separate self-attention branch, and upsample branch of ResTv2-T following [27]. As shown in Figure 3, the upsample module can indeed reconstruct the lost information, which mainly focuses on the medium- and high-frequency part, particularly in the earlier blocks. This aligns with our expectations since EMSAv2 downsamples the input with larger stride depth-wise convolutions in earlier blocks.

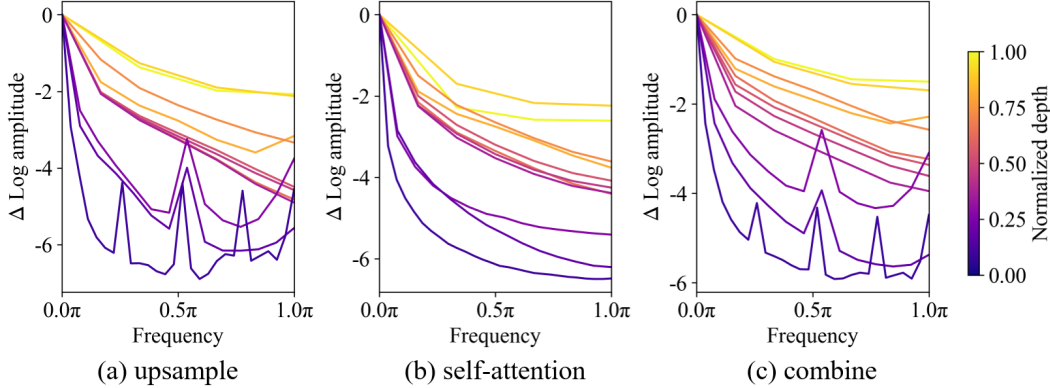


Figure 3: **Relative log amplitudes of Fourier transformed feature maps.** Δ Log amplitude is the difference between the log amplitude at normalized frequency 0.0π (center) and 1.0π (boundary).

4 Empirical Evaluations on ImageNet

4.1 Settings

The ImageNet-1k dataset consists of 1.28M training images and 50k validation images from 1,000 classes. We report the Top-1 and Top-5 accuracy on the validation set. We summarize our training and fine-tuning setups below. More details can be found in Appendix C.1.

We train ResTv2 for 300 epochs using AdamW [25], with a cosine decay learning rate scheduler and 50 epochs of linear warm-up. An initial learning rate of $1.5e-4 \times \text{batch_size} / 256$, a weight decay of 0.05, and gradient clipping with a max norm of 1.0 are used. For data augmentations, we adopt common schemes including Mixup [46], Cutmix [44], RandAugment [8], and Random Erasing [48]. We regularize the networks with Stochastic Depth [16] and Label Smoothing [32]. We use Exponential Moving Average (EMA) [29] as we find it alleviates larger models’ over-fitting. The default training and testing resolution is 224^2 . Additionally, we fine-tune at a large resolution of 384^2 , adopting AdamW for 30 epochs, with a learning rate $1.5e-5 \times \text{batch_size} / 256$, a cosine decaying schedule afterward, no warm up, and weight decay of $1e-8$.

4.2 Main Results

Table 1 shows the result comparison of the proposed ResTv2 with three recent Transformer variants, ResTv1 [47], Swin Transformer [23], and Focal Transformer [41], as well as two strong ConvNets: RegNet [30] and ConvNeXt [24].

ResTv2 competes favorably with them in terms of a speed-accuracy trade-off. Specifically, ResTv2 outperforms ResTv1 of similar complexities across the board, sometimes with a substantial margin, e.g., +0.7% (82.3% vs. 81.6%) in terms of Top-1 accuracy for ResTv2-T. Besides, ResTv2 outperforms the Focal counterparts with an average $\times 1.8$ inference throughput acceleration, although both of them share similar FLOPs. A highlight from the results is ResTv2-B: it outperforms Focal-S by +0.1% (83.7% vs. 83.6%), but with +203% higher inference throughput (582 vs. 192 images/s). ResTv2 also enjoys improved accuracy and throughput compared with similar-sized Swin Transformers, particularly for tiny models, the Top-1 accuracy improvement is +1.0% and (82.3% vs. 81.3%).

Table 1: **Classification accuracy on ImageNet-1k.** Inference throughput (images / s) is measured on a V100 GPU, following [47].

| Model | Image Size | Params | FLOPs | Throughput | Top-1 (%) | Top-5 (%) |
|------------------|------------------|--------|-------|-------------|-------------|-------------|
| RegNetY-4G [30] | 224 ² | 21M | 4.0G | 1156 | 79.4 | 94.7 |
| ConvNeXt-T [24] | 224 ² | 29M | 4.5G | 775 | 82.1 | 95.9 |
| Swin-T [23] | 224 ² | 28M | 4.5G | 755 | 81.3 | 95.5 |
| Focal-T [41] | 224 ² | 29M | 4.9G | 319 | 82.2 | 95.9 |
| ResTv1-B [47] | 224 ² | 30M | 4.3G | 673 | 81.6 | 95.7 |
| ResTv2-T | 224 ² | 30M | 4.1G | 826 | 82.3 | 95.5 |
| ResTv2-T | 384 ² | 30M | 12.7G | 319 | 83.7 | 96.6 |
| RegNetY-8G [30] | 224 ² | 39M | 8.0G | 591 | 79.9 | 94.9 |
| ResTv2-S | 224 ² | 41M | 6.0G | 687 | 83.2 | 96.1 |
| ResTv2-S | 384 ² | 41M | 18.4G | 256 | 84.5 | 96.7 |
| ConvNeXt-S [24] | 224 ² | 50M | 8.7G | 447 | 83.1 | 96.4 |
| Swin-S [23] | 224 ² | 50M | 8.7G | 437 | 83.2 | 96.2 |
| Focal-S [41] | 224 ² | 51M | 9.4G | 192 | 83.6 | 96.2 |
| ResTv1-L [47] | 224 ² | 52M | 7.9G | 429 | 83.6 | 96.3 |
| ResTv2-B | 224 ² | 56M | 7.9G | 582 | 83.7 | 96.3 |
| ResTv2-B | 384 ² | 56M | 24.3G | 210 | 85.1 | 97.2 |
| RegNetY-16G [30] | 224 ² | 84M | 15.9G | 334 | 80.4 | 95.1 |
| ConvNeXt-B [24] | 224 ² | 89M | 15.4G | 292 | 83.8 | 96.7 |
| Swin-B [23] | 224 ² | 88M | 15.4G | 278 | 83.5 | 96.5 |
| Focal-B [41] | 224 ² | 90M | 16.4G | 138 | 84.0 | 96.5 |
| ResTv2-L | 224 ² | 87M | 13.8G | 415 | 84.2 | 96.5 |
| ConvNeXt-B [24] | 384 ² | 89M | 45.0G | 96 | 85.1 | 97.3 |
| Swin-B [23] | 384 ² | 88M | 47.1G | 85 | 84.5 | 97.0 |
| ResTv2-L | 384 ² | 87M | 42.4G | 141 | 85.4 | 97.1 |

Additionally, we observe a highlight accuracy improvement when the resolution increases from 224² to 384². An average +1.4% Top-1 accuracy is achieved. We can conclude that the proposed ResTv2 also possesses the ability to scale up capacity and resolution.

4.3 Ablation Study

Here, we ablate essential design elements in ResTv2-T using ImageNet-1k image classification. To save computation energy, all experiments in this part are trained for 100 epochs, and 10 of them are applied for linear warm-up, with other settings unchanged.

Upsampling Targets. There are three options for upsampling, the output of down-sample operation x' , K, and V. Table 2(a) shows the results of upsampling these targets. Undoubtedly, upsampling K or V achieves better results than x' since K and V are obtained from x' via linear projection, enabling the communication of information between different features. Upsampling V works best. This can be attributed to the fact that unified modeling of the same variable (i.e., V) can better enhance the feature representation.

Upsampling Strategies. Table 2(b) varies the upsampling strategies. We can see that all of the three upsample strategies can increase the Top-1 accuracy, which means the upsample operation can provide information not captured by self-attention. In addition, pixel-shuffle operation obtains much stronger feature extraction capabilities with a few parameters and FLOPs increase.

ConvNet or EMSA? As mentioned in Section 3.2, we point out that the “downsampling-upsampling” pipeline in EMSAv2 can constitute a complete ConvNet block for extracting features. Here, we separate it (i.e., a ResTv2-T variant without self-attention) to see whether it can replace the MSA module in ViTs. Table 2(c) shows that with the same number of blocks, the performance of the ConvNet version is quite poor. In order to show that insufficient parameters and computation do not

Table 2: **Ablation experiments with ResTv2-T on ImageNet-1k.** If not specified, the default is: upsampling V using pixel-shuffle operation and applying PA as positional embedding. Default settings are marked in gray .

(a) **Upsampling Targets.** Upsampling V works the best.

| Targets | Top-1 (%) | Top-5 (%) |
|---------|--------------|--------------|
| w/o | 79.04 | 94.61 |
| x' | 79.64 | 94.90 |
| K | 80.03 | 94.95 |
| V | 80.33 | 95.06 |

(b) **Upsampling Strategies.** Pixel-Shuffle achieves better speed-accuracy trade-off.

| Upsample | Params | FLOPs | Top-1 (%) |
|---------------|---------------|--------------|--------------|
| w/o | 30.26M | 4.08G | 79.04 |
| nearest | 30.26M | 4.08G | 79.16 |
| bilinear | 30.26M | 4.08G | 79.28 |
| pixel-shuffle | 30.43M | 4.10G | 80.33 |

(c) **ConvNet or EMSA?** Both of them can boost the performance.

| Branches | Params | FLOPs | Top-1 (%) |
|-----------|---------------|--------------|--------------|
| EMSA | 30.26M | 4.08G | 79.04 |
| ConvNet | 26.11M | 3.56G | 77.18 |
| ConvNetv2 | 26.67M | 4.09G | 77.91 |
| EMSAv2 | 30.43M | 4.10G | 80.33 |

(d) **Positional Embedding.** Both RPE and PA work well, but PA is more flexible.

| PE | Params | Top-1 (%) |
|----------|---------------|--------------|
| w/o | 30.42M | 79.94 |
| APE [11] | 30.98M | 79.99 |
| RPE [31] | 30.48M | 80.32 |
| PA [47] | 30.43M | 80.33 |

mainly cause this issue, we constructed ConvNetv2, i.e., adding a block in both the first and second stages, so that the model complexity of the ConvNetv2 and EMSA versions (without upsample) is equivalent. Experimental results show that ConvNetv2 still performs inferior to the EMSA version (77.91 vs. 79.04 in terms of Top-1 accuracy). This observation indicates that ConvNet does not act like EMSA. Thus, it is not reasonable to replace MSA with ConvNet in ViTs.

However, combining the upsample module and EMSA (i.e., EMSAv2) indeed improves the overall performance. We can conclude that the downsampling operation of EMSAv2 will lead to the loss of input information, resulting in insufficient information extracted by the EMSA module constructed on this basis, and the upsample operation can reconstruct the lost information.

We further plot the linear CKA [18] curves to measure which is more critical for EMSAv2 (i.e., the combination variant), the self-attention branch (i.e., EMSA) or the upsample module? Figure 4 illustrates that in earlier blocks, feature representations extracted by self-attention and upsample module show a relatively low similarity, while in deeper blocks, they exhibit a surprisingly high similarity (shown in the red polyline). We can conclude that features in earlier blocks extracted by self-attention and upsample module are complementary. Combining them can boost the final performance. In deeper blocks, particularly the last block, self-attention behaves like the upsample module (linear CKA > 0.8), although it shows a higher similarity with EMSAv2 (shown in the purple polyline). These observations could provide a guide for designing hybrid models, i.e., integrating ConvNets and MSAs in the early stages can significantly improve the performance of ViTs.

Positional Embedding. We also validate whether Positional Embedding (short for PE) still works in ResTv2.

Table 2(d) shows PE can still improve the performance, but not that obvious as ResTv1 [47]. Specifically, both RPE and PA work well, but PA is more flexible, which can process input images of

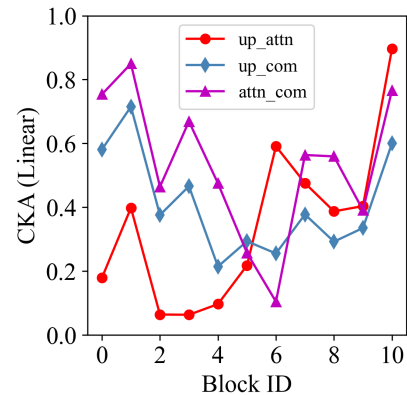


Figure 4: **Linear CKA Similarity** between EMSA, Upsample and EMSAv2 with ResTv2-T.

arbitrary size without interpolation or fine-tuning. Therefore, we apply PA as the default PE strategy. Detailed settings about these positional embedding can be found in Appendix E.

5 Empirical Evaluation on Downstream Tasks

5.1 Object Detection and Segmentation on COCO

Settings. Object detection and instance segmentation experiments are conducted on COCO 2017, which contains 118K training, 5K validation, and 20K test-dev images. We report results using the validation set. We fine-tune Mask R-CNN [14] with ResTv2 backbones. Following [24], we adopt multi-scale training, AdamW optimizer, “ $\times 1$ schedule” for ablation study, and “ $\times 3$ schedule” for main results. Further details and hyper-parameter settings can be found in Appendix C.2.

Ablation Study. There are several ways to fine-tune ImageNet pre-trained ViT backbones. The conventional one is the global style, which directly adopts ViTs into downstream tasks. The recent popular one is window-style (short for Win), which constrained part or all MSA modules of ViTs into a fixed window to save computation overhead. However, performing all MSA into a limited-sized window will lose the MSA’s long-range dependency ability. To alleviate this issue, we add a 7×7 depth-wise convolution layer after the last block in each stage to enable information to communicate across windows. We call this style CWin. In addition, [20] provides a hybrid approach (HWin) to integrate window information, i.e., computes MSA within a window in all but the last blocks in each stage that feed into FPN [21]. Window sizes in Win, CWin, and HWin are set as [64, 32, 16, 8] for the four stages.

Table 3: **Object detection results of fine-tuning styles on COCO val2017 with ResTv2-T using Mask RCNN.** Inference “ms/iter” is measured on a V100 GPU, and FLOPs are calculated with 1k validation images.

| (a) Object detection results. | | | | | | (b) Detailed GFLOPs Analysis | | | | |
|-------------------------------|---------|--------|-------------|-------------------|--------------------|------------------------------|--------|--------|--------|--------|
| Style | Params. | FLOPs | ms/iter | AP ^{box} | AP ^{mask} | Style | Conv | Linear | Matmul | Others |
| Win | 49.94M | 205.2G | 149.6 | 43.95 | 40.42 | Win | 119.09 | 82.00 | 3.69 | 0.47 |
| CWin | 49.96M | 212.5G | 150.7 | 44.07 | 40.44 | CWin | 126.29 | 82.00 | 3.69 | 0.47 |
| HWin | 49.94M | 218.9G | 135.9 | 45.02 | 41.56 | HWin | 118.57 | 79.71 | 20.17 | 0.45 |
| Global | 49.94M | 229.7G | 79.9 | 46.13 | 42.03 | Global | 116.95 | 75.70 | 36.66 | 0.42 |

Table 3(a) shows that although restricted EMSAv2 into fixed windows can effectively reduce theoretical FLOPs, the actual inference speed is almost double the global style, and the box/mask AP is lower than the global one. Therefore, we adopt the Global fine-tuning strategy as default in downstream tasks to get better accuracy and inference speed.

There are mainly two reasons for the decrease in inference speed: (1) padding to inputs is required to satisfy the divisible non-overlapped window partition. In our settings, the theoretical upper limit of padding in the first stage is 63×63 , close to the lower bound of the input features’ size (i.e., 64×64). (2) the process of window partition is similar to feature grouping, which reduces the computational density of GPUs.

Table 3(b) shows the detailed FLOPs of different modules. We can see that window-based fine-tune methods can effectively reduce the “Matmul” (short of matrix multiply) FLOPs with the cost of introducing extra “Linear” FLOPs, demonstrating that window partition padding is common in detection tasks. In addition, the “Matmul” operation is not the most time-consuming part of the four settings ($\leq 16\%$). Therefore, it is reasonable to speculate that window attention will reduce computational density.

We hope the observations and discussions can challenge some common beliefs and encourage people to rethink the relations between theoretical FLOPs and actual speeds, particularly running on GPUs.

Main Results. Table 4 shows main results of ResTv2 comparing with ConvNeXt [24], Swin Transformer [23], and traditional ConvNet such as ResNet [15]. Across different model complexities,

Table 4: **COCO object detection and segmentation results using Mask-RCNN**. We measure FPS on one V100 GPU. FLOPs are calculated with image size (1280, 800).

| Backbones | AP ^{box} | AP ^{mask} | Params. | FLOPs | FPS |
|-----------------|-------------------|--------------------|---------|-------|-------------|
| ResNet-50 [15] | 41.0 | 37.1 | 44.2M | 260G | 24.1 |
| ConvNeXt-T [24] | 46.2 | 41.7 | 48.1M | 262G | 23.4 |
| Swin-T [23] | 46.0 | 41.6 | 47.8M | 264G | 21.8 |
| ResTv2-T | 47.6 | 43.2 | 49.9M | 253G | 25.0 |
| ResNet-101 [15] | 42.8 | 38.5 | 63.2M | 336G | 13.5 |
| Swin-S [23] | 48.5 | 43.3 | 69.1M | 354G | 17.4 |
| ResTv2-S | 48.1 | 43.3 | 60.7M | 290G | 21.3 |
| ResTv2-B | 48.7 | 43.9 | 75.5M | 328G | 18.3 |

ResTv2 outperforms Swin Transformer and ConvNeXt with higher mAP and inference FPS (frames per second), particularly for tiny models. The mAP improvements over Swin Transformer are +1.6 box AP (47.6 vs. 46.0), and +1.6 mask AP (43.2 vs. 41.6). When comparing with ConvNeXt, the improvements are +1.4 box AP (47.6 vs. 46.2), and +1.5 mask AP (43.2 vs. 41.7).

5.2 Semantic Segmentation on ADE20K

Settings. We also evaluate ResTv2 backbones on the ADE20K [49] semantic segmentation task with UperNet [39]. ADE20K contains a broad range of 150 semantic categories. It has 25K images in total, with 20K for training, 2K for validation, and another 3K for testing. All model variants are trained for 160k iterations with a batch size of 16. Other experimental settings follow [23] (see Appendix C.2 for more details).

Table 5: **ADE20K validation results using UperNet**. Following Swin, we report mIoU results with multiscale testing. FLOPs are based on input sizes of (2048, 512).

| Backbones | input crop. | mIoU | Params. | FLOPs | FPS |
|-----------------|------------------|-------------|---------|-------|-------------|
| ResNet-50 [15] | 512 ² | 42.8 | 66.5M | 952G | 23.4 |
| ConvNeXt-T [24] | 512 ² | 46.7 | 60.2M | 939G | 19.9 |
| Swin-T [23] | 512 ² | 45.8 | 59.9 M | 941G | 21.1 |
| ResTv2-T | 512 ² | 47.3 | 62.1M | 977G | 22.4 |
| ResNet-101 [15] | 512 ² | 44.9 | 85.5M | 1029G | 20.3 |
| ConvNeXt-S [24] | 512 ² | 49.0 | 81.9M | 1027G | 15.3 |
| Swin-S [23] | 512 ² | 49.2 | 81.3M | 1038G | 14.7 |
| ResTv2-S | 512 ² | 49.2 | 72.9M | 1035G | 20.0 |
| ResTv2-B | 512 ² | 49.6 | 87.6M | 1095G | 19.2 |

Results. In Table 5, we report validation mIoU with multi-scale testing. ResTv2 models can achieve competitive performance across different model capacities, further validating the effectiveness of our architecture design. Specifically, ResTv2-T outperforms Swin-T and ConvNeXt-T with +1.5 and +0.7 mIoU improvements, respectively (47.3 vs. 45.8 vs. 46.7) with much higher FPS (22.4 vs. 21.1 vs. 19.9 images/s). As for larger models, the mIoU improvements of ResTv2-B over Swin-S and ConvNeXt-B are +0.4 and +0.6 (49.6 vs. 49.2 vs. 49.0). The inference speed improvements are +30.6% and +25.5% (19.2 vs. 14.7 vs. 15.3 images/s).

6 Conclusion

In this paper, we proposed ResTv2, a simpler, faster, and stronger multi-scale vision Transformer for image recognition. ResTv2 adopts pixel-shuffle in EMSAv2 to reconstruct the lost information due to the downsampling operation. In addition, we explore different techniques for better apply ResTv2 to downstream tasks. Results show that the theoretical FLOPs is not a good reflection of actual speed,

particularly running on GPUs. We hope that these observations could encourage people to rethink architecture design techniques that can actually prompt the network’s efficiency.

Acknowledgments and Disclosure of Funding

This work is funded by the Natural Science Foundation of China (No. 62176119). We thank many colleagues at Nanjing University for their help, particularly Rao Lu, Niu Zhong-Han, and Xu Jian, for useful discussion and the help on GPU resources.

A Comparison with different MSA variants.

This section provides more results about the effectiveness of the upsampling operation in different MSA variants under 100 training epochs settings following Section 4.3. As shown in Table 6, MSA variants with the “downsample-upsample” branch can compete favorably with the standard MSA in terms of the Top-1 accuracy but with much higher inference throughput.

Table 6: **Results of different MSAs.** \dagger means the implementation of adding an upsample operation for SRA[35] or EMSA[47], and $*$ means replacing SRA or EMSA with the standard MSA, leaving other components unchanged. Inference throughput (images / s) is measured on a V100 GPU, following [47].

| Methods | Params | FLOPs | Throughput | Top-1 (%) |
|------------------------------|--------|-------|------------|--------------|
| PVT-Tiny[35] | 13.27M | 1.94G | 1144 | 70.46 |
| PVT-MSA-Tiny $*$ | 11.36M | 4.81G | 617 | 72.38 |
| PVT-EMSAv2-Tiny \dagger | 13.95M | 1.95G | 947 | 72.53 |
| ResTv1-Lite[47] | 10.50M | 1.44G | 1091 | 74.108 |
| ResTv1-MSA-Lite $*$ | 10.48M | 4.37G | 625 | 75.06 |
| ResTv1-EMSAv2-Lite \dagger | 10.66M | 1.45G | 926 | 75.04 |

B Results of Multi-head Interaction Module

In this section, we estimate the role of the Multi-head Interaction Module (short for MHIM). Training settings are the same as Section 4.3, i.e., under the 100 training epochs settings. As shown in Table 7, MHIM can significantly improve the Top-1 accuracy with the cost of decreased inference throughput when the channel dimension of each head d_k is smaller. When d_k is larger (e.g., 96), the accuracy improvement is limited. Therefore, we may choose whether to apply MHIM in EMSAv2 according to different scenarios.

Table 7: **Results of short for MHIM.** ResTv2-Lite is a shallow ResTv2 variant with blocks number={2, 2, 2, 2} and $C = 64$. Inference throughput (images / s) is measured on a V100 GPU, following [47].

| Methods | head_dim | Params | FLOPs | Throughput | Top-1 (%) |
|-------------|----------|---------|-------|------------|---------------|
| ResTv2-Lite | 64 | 10.66M | 1.45G | 945 | 74.54 |
| +MHIM | 64 | 10.66M | 1.45G | 926(-19) | 75.04(+0.5) |
| ResTv2-Tiny | 96 | 30.43 M | 4.10G | 826 | 80.33 |
| +MHIM | 96 | 30.44M | 4.10G | 792(-34) | 80.47 (+0.14) |

C Experimental Settings

C.1 ImageNet pre-training and finetuning settings

We list the settings for training and fine-tuning on ImageNet-1k in Table 8. The settings are used for our main results in Table 1 (Section 4.2). The fine-tuning starts from the best checkpoint weights obtained in pre-training.

Table 8: **ImageNet-1k training and fine-tuning settings.** Multiple stochastic depth rates (e.g., 0.1/0.2/0.3/0.5) are for each model (e.g., ResTv2-T/S/B/L) respectively.

| configure | pre-training | fine-tuning |
|------------------------|----------------------------------|----------------------------------|
| input crop. | 224 ² | 384 ² |
| optimizer | AdamW | AdamW |
| base learning rate | 1.5e-4 | 1.5e-5 |
| weight decay | 0.05 | 1e-8 |
| optimizer momentum | $\beta_1 = 0.9, \beta_2 = 0.999$ | $\beta_1 = 0.9, \beta_2 = 0.999$ |
| batch size | 2048 | 512 |
| training epoch | 300 | 30 |
| learning rate schedule | cosine decay | cosine decay |
| warmup epochs | 50 | N/A |
| warmup schedule | linear | N/A |
| RandAugment [8] | (9, 0.5) | (9, 0.5) |
| label smoothing [32] | 0.1 | 0.1 |
| Mixup [46] | 0.8 | N/A |
| Cutmix [44] | 1.0 | N/A |
| stochastic depth [16] | 0.1/0.2/0.3/0.5 | 0.1/0.2/0.3/0.5 |
| gradient clip | 1.0 | 1.0 |
| EMA [29] | 0.9999 | N/A |

C.2 Downstream Tasks.

For COCO and ADE20K experiments, we follow the training settings used in ResTv1 [47] and ConvNeXt [24]. We adopt Detectron2 [37] toolboxes for object detection, and MMSegmentation [7] toolboxes for semantic segmentation. We use the best model weights (instead of EMA weights) from ImageNet pre-training as network initialization.

Object Detection on COCO. We utilize multi-scale training, i.e., resizing the input such that the short side is between 480 and 800 while the longer side is at most 1333, AdamW optimizer with initial learning rate of 0.0001, weight decay of 0.05, and batch size of 16 (8 V100 GPUs with two images per GPU), “ $\times 1$ ” schedule (90K iterations with learning rate decayed by $\times 10$ at 60K and 80K steps) for ablation study, and “ $\times 3$ ” schedule (270K iterations with learning rate decayed by $\times 10$ at 210K and 250K steps) for main results. We apply standard data augmentation, that is resize, random flip and normalize. Additionally, we adopt stochastic depth with ratio of 0.1/0.2/0.3 for ResTv2-T/S/B. All results are reported on the validation set.

Semantic segmentation on ADE20K. We employ the AdamW optimizer with an initial learning rate of 1.5e-4, a weight decay of 0.05, stage-wise learning rate decay with a ratio of 0.9, and a linear warmup of 1,500 iterations. Models are trained on 8 GPUs with two images per GPU for 160K iterations. Stochastic depth with ratio of 0.1/0.2/0.3 for ResTv2-T/S/B. All models are trained on the standard setting with an input of 512×512 . We report validation mIoU results using multi-scale testing.

D Detailed Architectures

The detailed architecture specifications are shown in Table 9, where an input image size of 224×224 is assumed for all architectures. “Conv- K _ C _ S ” means convolution layers with kernel size K , output channel C and stride S . “MLP_ C ” is the FFN layer with hidden channel $4C$ and output channel C . “Ev2_ H _ R ” is the EMSAv2 operation with the number of heads H and reduction ratio R . “C” is 96 for ResTv2-T/S/B, and 128 for ResTv2-L. “PA” [47] is short for pixel-wise attention.

Table 9: **Detailed architecture specifications.** FLOPs are calculated with image size (224, 224).

| Module | Output | ResTv2-T | ResTv2-S | ResTv2-B | ResTv2-L |
|------------|----------------|--|---|---|--|
| stem | 56×56 | Patch Embedding: Conv-3_C/2_2, Conv-3_C_2, Conv-1_C_1, PA | | | |
| stage1 | 56×56 | $\begin{bmatrix} \text{Ev2_1_8} \\ \text{MLP_96} \end{bmatrix} \times 1$ | $\begin{bmatrix} \text{Ev2_1_8} \\ \text{MLP_96} \end{bmatrix} \times 1$ | $\begin{bmatrix} \text{Ev2_1_8} \\ \text{MLP_96} \end{bmatrix} \times 1$ | $\begin{bmatrix} \text{Ev2_2_8} \\ \text{MLP_128} \end{bmatrix} \times 2$ |
| | | Patch Embedding: Conv-3_2C_2, PA | | | |
| stage2 | 28×28 | $\begin{bmatrix} \text{Ev2_2_4} \\ \text{MLP_192} \end{bmatrix} \times 2$ | $\begin{bmatrix} \text{Ev2_2_4} \\ \text{MLP_192} \end{bmatrix} \times 2$ | $\begin{bmatrix} \text{Ev2_2_4} \\ \text{MLP_192} \end{bmatrix} \times 3$ | $\begin{bmatrix} \text{Ev2_4_4} \\ \text{MLP_256} \end{bmatrix} \times 3$ |
| | | Patch Embedding: Conv-3_4C_2, PA | | | |
| stage3 | 14×14 | $\begin{bmatrix} \text{Ev2_4_2} \\ \text{MLP_384} \end{bmatrix} \times 6$ | $\begin{bmatrix} \text{Ev2_4_2} \\ \text{MLP_384} \end{bmatrix} \times 12$ | $\begin{bmatrix} \text{Ev2_4_2} \\ \text{MLP_384} \end{bmatrix} \times 16$ | $\begin{bmatrix} \text{Ev2_8_2} \\ \text{MLP_512} \end{bmatrix} \times 16$ |
| | | Patch Embedding: Conv-3_8C_2, PA | | | |
| stage4 | 7×7 | $\begin{bmatrix} \text{Ev2_8_1} \\ \text{MLP_768} \end{bmatrix} \times 2$ | $\begin{bmatrix} \text{Ev2_8_1} \\ \text{MLP_768} \end{bmatrix} \times 2$ | $\begin{bmatrix} \text{Ev2_8_1} \\ \text{MLP_768} \end{bmatrix} \times 3$ | $\begin{bmatrix} \text{Ev2_16_1} \\ \text{MLP_1024} \end{bmatrix} \times 2$ |
| Classifier | | Average Pooling, 1000D Fully-Connected Layer | | | |
| FLOPs | | 4.0G | 5.8G | 7.7G | 13.5G |

E Positional Embedding

In Section 4.3, we explore three types of positional embedding in ResTv2. Here, we give the mathematical definition of them. Assume $x \in \mathbb{R}^{hw \times d_m}$ be the input token sequence, where h , w and d_m are the input’s height, width and channel dimensions, respectively.

APE. Let $\theta \in \mathbb{R}^{n \times c}$ be position parameters, then APE[11] can be represented as

$$\hat{x} = x + \theta \quad (3)$$

In APE, θ should be the same size as the input x , i.e., $n = h \cdot w$, whatever θ is sinusoidal or learnable.

RPE. RPE applied in this paper is the relative position variant introduced in [31], which is added to the attention map to represent the structure of inputs (i.e., 2D images). Let Q be the queries, K be the keys, k be the number of heads, and d_k be the head dimension. Then position P can be obtained by $P = P_h + P_w$, where $P_h \in \mathbb{R}^{k \times h' \times 1 \times d_k}$ and $P_w \in \mathbb{R}^{k \times 1 \times w' \times d_k}$ represent the positions along the height dimension and the width dimension, respectively. The RPE can then be defined as:

$$\text{Attn}(Q, K) = \text{Softmax}\left(\frac{Q(K + P)^T}{\sqrt{d_k}}\right) \quad (4)$$

Therefore, RPE can capture both the “content-content” and “content-position” information. However, P is required to share the same resolution as K , i.e., $h' = h, w' = w$ in the standard MSA, and $h' = h/r, w' = w/r$ in EMSAv2, where r is the reduction factor.

PA. PA is one kind of spatial attention that utilizes a simple 2D depth-wise convolution as the transform function [47]. Thanks to the shared parameters and locality of convolution, PA can tackle arbitrary lengths of inputs and capture their absolute positions with the help of zero paddings. The mathematical formulation of PA can be defined as

$$\text{PA}(x) = x \cdot \sigma(\text{DWConv}(x)) \quad (5)$$

where $\sigma(\cdot)$ is the sigmoid function adopted to scale the spatial attention weights.

References

- [1] Jimmy Lei Ba, Jamie Ryan Kiros, and Geoffrey E Hinton. Layer normalization. *arXiv preprint arXiv:1607.06450*, 2016.
- [2] Nicolas Carion, Francisco Massa, Gabriel Synnaeve, Nicolas Usunier, Alexander Kirillov, and Sergey Zagoruyko. End-to-end object detection with transformers. In *European conference on computer vision, ECCV2020*, pages 213–229. Springer, 2020.
- [3] Hanting Chen, Yunhe Wang, Tianyu Guo, Chang Xu, Yiping Deng, Zhenhua Liu, Siwei Ma, Chunjing Xu, Chao Xu, and Wen Gao. Pre-trained image processing transformer. In *IEEE Conference on Computer Vision and Pattern Recognition, CVPR 2021*, pages 12299–12310. Computer Vision Foundation / IEEE, 2021.
- [4] Yinpeng Chen, Xiyang Dai, Dongdong Chen, Mengchen Liu, Xiaoyi Dong, Lu Yuan, and Zicheng Liu. Mobile-former: Bridging mobilenet and transformer. In *International Conference on Computer Vision and Pattern Recognition, CVPR 2022*, 2022.
- [5] Xiangxiang Chu, Zhi Tian, Yuqing Wang, Bo Zhang, Haibing Ren, Xiaolin Wei, Huaxia Xia, and Chunhua Shen. Twins: Revisiting the design of spatial attention in vision transformers. In A. Beygelzimer, Y. Dauphin, P. Liang, and J. Wortman Vaughan, editors, *Advances in Neural Information Processing Systems, NeurIPS 2021*, 2021.
- [6] Xiangxiang Chu, Bo Zhang, Zhi Tian, Xiaolin Wei, and Huaxia Xia. Conditional positional encodings for vision transformers. *arXiv preprint arXiv:2102.10882*, 2021.
- [7] MMSegmentation Contributors. MMsegmentation: Openmmlab semantic segmentation toolbox and benchmark. <https://github.com/open-mmlab/mmsegmentation>, 2020.
- [8] Ekin Dogus Cubuk, Barret Zoph, Jon Shlens, and Quoc Le. Randaugment: Practical automated data augmentation with a reduced search space. In *Advances in Neural Information Processing Systems, NeurIPS 2020*, 2020.
- [9] Zihang Dai, Hanxiao Liu, Quoc V Le, and Mingxing Tan. Coatnet: Marrying convolution and attention for all data sizes. In A. Beygelzimer, Y. Dauphin, P. Liang, and J. Wortman Vaughan, editors, *Advances in Neural Information Processing Systems, NeurIPS 2021*, 2021.
- [10] Xiaoyi Dong, Jianmin Bao, Dongdong Chen, Weiming Zhang, Nenghai Yu, Lu Yuan, Dong Chen, and Baining Guo. Cswin transformer: A general vision transformer backbone with cross-shaped windows. In *Proceedings of the IEEE/CVF Conference on Computer Vision and Pattern Recognition, CVPR 2022*, 2022.
- [11] Alexey Dosovitskiy, Lucas Beyer, Alexander Kolesnikov, Dirk Weissenborn, Xiaohua Zhai, Thomas Unterthiner, Mostafa Dehghani, Matthias Minderer, Georg Heigold, Sylvain Gelly, Jakob Uszkoreit, and Neil Houlsby. An image is worth 16x16 words: Transformers for image recognition at scale. In *9th International Conference on Learning Representations, ICLR 2021*. OpenReview.net, 2021.
- [12] Haoqi Fan, Bo Xiong, Karttikeya Mangalam, Yanghao Li, Zhicheng Yan, Jitendra Malik, and Christoph Feichtenhofer. Multiscale vision transformers. In *2021 IEEE/CVF International Conference on Computer Vision, ICCV 2021*, pages 6804–6815. IEEE, 2021.
- [13] Kaiming He, Xinlei Chen, Saining Xie, Yanghao Li, Piotr Dollár, and Ross Girshick. Masked autoencoders are scalable vision learners. In *International Conference on Computer Vision and Pattern Recognition, CVPR 2022*, 2022.
- [14] Kaiming He, Georgia Gkioxari, Piotr Dollár, and Ross B. Girshick. Mask R-CNN. In *IEEE International Conference on Computer Vision, ICCV 2017*, pages 2980–2988. IEEE Computer Society, 2017.
- [15] Kaiming He, Xiangyu Zhang, Shaoqing Ren, and Jian Sun. Deep residual learning for image recognition. In *2016 IEEE Conference on Computer Vision and Pattern Recognition, CVPR 2016*, pages 770–778. IEEE Computer Society, 2016.
- [16] Gao Huang, Yu Sun, Zhuang Liu, Daniel Sedra, and Kilian Q. Weinberger. Deep networks with stochastic depth. In *14th European Conference on Computer Vision, ECCV 2016*, volume 9908, pages 646–661. Springer, 2016.
- [17] Zilong Huang, Youcheng Ben, Guozhong Luo, Pei Cheng, Gang Yu, and Bin Fu. Shuffle transformer: Rethinking spatial shuffle for vision transformer. *arXiv preprint arXiv:2106.03650*, 2021.
- [18] Simon Kornblith, Mohammad Norouzi, Honglak Lee, and Geoffrey E. Hinton. Similarity of neural network representations revisited. In *Proceedings of the 36th International Conference on Machine Learning, ICML 2019*, volume 97, pages 3519–3529. PMLR, 2019.
- [19] Kunchang Li, Yali Wang, Gao Peng, Guanglu Song, Yu Liu, Hongsheng Li, and Yu Qiao. Uniformer: Unified transformer for efficient spatial-temporal representation learning. In *International Conference on Learning Representations, ICLR 2022*, 2022.
- [20] Yanghao Li, Chao-Yuan Wu, Haoqi Fan, Karttikeya Mangalam, Bo Xiong, Jitendra Malik, and Christoph Feichtenhofer. Improved multiscale vision transformers for classification and detection. *arXiv preprint arXiv:2112.01526*, 2021.
- [21] Tsung-Yi Lin, Piotr Dollár, Ross B. Girshick, Kaiming He, Bharath Hariharan, and Serge J. Belongie. Feature pyramid networks for object detection. In *2017 IEEE Conference on Computer Vision and Pattern Recognition, CVPR 2017*, pages 936–944, 2017.
- [22] Ze Liu, Han Hu, Yutong Lin, Zhuliang Yao, Zhenda Xie, Yixuan Wei, Jia Ning, Yue Cao, Zheng Zhang, Li Dong, et al. Swin transformer v2: Scaling up capacity and resolution. In *Proceedings of the IEEE/CVF Conference on Computer Vision and Pattern Recognition, CVPR 2022*, 2022.

[23] Ze Liu, Yutong Lin, Yue Cao, Han Hu, Yixuan Wei, Zheng Zhang, Stephen Lin, and Baining Guo. Swin transformer: Hierarchical vision transformer using shifted windows. In *2021 IEEE/CVF International Conference on Computer Vision, ICCV 2021*, pages 9992–10002. IEEE, 2021.

[24] Zhuang Liu, Hanzi Mao, Chao-Yuan Wu, Christoph Feichtenhofer, Trevor Darrell, and Saining Xie. A convnet for the 2020s. In *Proceedings of the IEEE/CVF Conference on Computer Vision and Pattern Recognition, CVPR 2022*, 2022.

[25] Ilya Loshchilov and Frank Hutter. Decoupled weight decay regularization. In *7th International Conference on Learning Representations, ICLR 2019*. OpenReview.net, 2019.

[26] Xuran Pan, Chunjiang Ge, Rui Lu, Shiji Song, Guanfu Chen, Zeyi Huang, and Gao Huang. On the integration of self-attention and convolution. In *Proceedings of the IEEE/CVF Conference on Computer Vision and Pattern Recognition, CVPR 2022*, 2022.

[27] Namuk Park and Songkuk Kim. How do vision transformers work? In *International Conference on Learning Representations, ICLR 2022*, 2022.

[28] Zhiliang Peng, Wei Huang, Shanzhi Gu, Lingxi Xie, Yaowei Wang, Jianbin Jiao, and Qixiang Ye. Conformer: Local features coupling global representations for visual recognition. In *2021 IEEE/CVF International Conference on Computer Vision, ICCV 2021*, pages 357–366. IEEE, 2021.

[29] Boris T Polyak and Anatoli B Juditsky. Acceleration of stochastic approximation by averaging. *SIAM journal on control and optimization*, 30(4):838–855, 1992.

[30] Ilija Radosavovic, Raj Prateek Kosaraju, Ross B. Girshick, Kaiming He, and Piotr Dollár. Designing network design spaces. In *2020 IEEE/CVF Conference on Computer Vision and Pattern Recognition, CVPR 2020*, pages 10425–10433. IEEE, 2020.

[31] Aravind Srinivas, Tsung-Yi Lin, Niki Parmar, Jonathon Shlens, Pieter Abbeel, and Ashish Vaswani. Bottleneck transformers for visual recognition. In *IEEE Conference on Computer Vision and Pattern Recognition, CVPR 2021*, pages 16519–16529. Computer Vision Foundation / IEEE, 2021.

[32] Christian Szegedy, Vincent Vanhoucke, Sergey Ioffe, Jonathon Shlens, and Zbigniew Wojna. Rethinking the inception architecture for computer vision. In *2016 IEEE Conference on Computer Vision and Pattern Recognition, CVPR 2016*, pages 2818–2826. IEEE Computer Society, 2016.

[33] Dmitry Ulyanov, Andrea Vedaldi, and Victor S. Lempitsky. Instance normalization: The missing ingredient for fast stylization. *arXiv preprint arXiv:1607.08022*, 2016.

[34] Ashish Vaswani, Noam Shazeer, Niki Parmar, Jakob Uszkoreit, Llion Jones, Aidan N. Gomez, Łukasz Kaiser, and Illia Polosukhin. Attention is all you need. In *Advances in Neural Information Processing Systems, NeurIPS 2017*, pages 5998–6008, 2017.

[35] Wenhui Wang, Enze Xie, Xiang Li, Deng-Ping Fan, Kaitao Song, Ding Liang, Tong Lu, Ping Luo, and Ling Shao. Pyramid vision transformer: A versatile backbone for dense prediction without convolutions. In *2021 IEEE/CVF International Conference on Computer Vision, ICCV 2021*, pages 548–558. IEEE, 2021.

[36] Haiping Wu, Bin Xiao, Noel Codella, Mengchen Liu, Xiyang Dai, Lu Yuan, and Lei Zhang. CvT: Introducing convolutions to vision transformers. In *2021 IEEE/CVF International Conference on Computer Vision, ICCV 2021*, pages 22–31. IEEE, 2021.

[37] Yuxin Wu, Alexander Kirillov, Francisco Massa, Wan-Yen Lo, and Ross Girshick. Detectron2. <https://github.com/facebookresearch/detectron2>, 2019.

[38] Tete Xiao, Piotr Dollar, Mannat Singh, Eric Mintun, Trevor Darrell, and Ross Girshick. Early convolutions help transformers see better. In A. Beygelzimer, Y. Dauphin, P. Liang, and J. Wortman Vaughan, editors, *Advances in Neural Information Processing Systems, NeurIPS 2017*, 2021.

[39] Tete Xiao, Yingcheng Liu, Bolei Zhou, Yuning Jiang, and Jian Sun. Unified perceptual parsing for scene understanding. In *15th European Conference on Computer Vision, ECCV 2018*, volume 11209, pages 432–448. Springer, 2018.

[40] Zhenda Xie, Zheng Zhang, Yue Cao, Yutong Lin, Jianmin Bao, Zhuliang Yao, Qi Dai, and Han Hu. Simmim: A simple framework for masked image modeling. In *International Conference on Computer Vision and Pattern Recognition, CVPR 2022*, 2022.

[41] Jianwei Yang, Chunyuan Li, Pengchuan Zhang, Xiyang Dai, Bin Xiao, Lu Yuan, and Jianfeng Gao. Focal attention for long-range interactions in vision transformers. In A. Beygelzimer, Y. Dauphin, P. Liang, and J. Wortman Vaughan, editors, *Advances in Neural Information Processing Systems, NeurIPS 2021*, 2021.

[42] Qihang Yu, Yingda Xia, Yutong Bai, Yongyi Lu, Alan Yuille, and Wei Shen. Glance-and-gaze vision transformer. In A. Beygelzimer, Y. Dauphin, P. Liang, and J. Wortman Vaughan, editors, *Advances in Neural Information Processing Systems, NeurIPS 2021*, 2021.

[43] Li Yuan, Yunpeng Chen, Tao Wang, Weihao Yu, Yujun Shi, Zihang Jiang, Francis E. H. Tay, Jiashi Feng, and Shuicheng Yan. Tokens-to-token vit: Training vision transformers from scratch on imagenet. In *2021 IEEE/CVF International Conference on Computer Vision, ICCV 2021*, pages 538–547. IEEE, 2021.

[44] Sangdoo Yun, Dongyoon Han, Sanghyuk Chun, Seong Joon Oh, Youngjoon Yoo, and Junsuk Choe. Cutmix: Regularization strategy to train strong classifiers with localizable features. In *2019 IEEE/CVF International Conference on Computer Vision, ICCV 2019*, pages 6022–6031. IEEE, 2019.

[45] Xiaohua Zhai, Alexander Kolesnikov, Neil Houlsby, and Lucas Beyer. Scaling vision transformers. *arXiv preprint arXiv:2106.04560*, 2021.

[46] Hongyi Zhang, Moustapha Cissé, Yann N. Dauphin, and David Lopez-Paz. mixup: Beyond empirical risk minimization. In *6th International Conference on Learning Representations, ICLR 2018*. OpenReview.net, 2018.

- [47] Qinglong Zhang and Yu bin Yang. Rest: An efficient transformer for visual recognition. In A. Beygelzimer, Y. Dauphin, P. Liang, and J. Wortman Vaughan, editors, *Advances in Neural Information Processing Systems, NeurIPS 2021*, 2021.
- [48] Zhun Zhong, Liang Zheng, Guoliang Kang, Shaozi Li, and Yi Yang. Random erasing data augmentation. In *The Thirty-Fourth AAAI Conference on Artificial Intelligence, AAAI 2020*, pages 13001–13008. AAAI Press, 2020.
- [49] Bolei Zhou, Hang Zhao, Xavier Puig, Tete Xiao, Sanja Fidler, Adela Barriuso, and Antonio Torralba. Semantic understanding of scenes through the ADE20K dataset. *Int. J. Comput. Vis.*, 127(3):302–321, 2019.
- [50] Xizhou Zhu, Weijie Su, Lewei Lu, Bin Li, Xiaogang Wang, and Jifeng Dai. Deformable DETR: deformable transformers for end-to-end object detection. In *9th International Conference on Learning Representations, ICLR 2021*. OpenReview.net, 2021.